

The Effect Manganese Concentration on the Corrosion Resistance and Physical Properties of Zn-Ni-Mn Alloy Films Produced by Electrodeposition

Fawzi H. Assaf¹, Mortaga M. Abou-Krishna^{1,3,*}, Omar k. Alduaij³,
Ahmed M. A. El-Seidy^{2,3} and Ahmed A. Eissa¹

¹Faculty of Science, Chemistry Department, South Valley University, Qena, 83523, Egypt.

²Inorganic Chemistry Department, National Research Centre, P.O. 12622, Dokki, Giza, Egypt.

³College of Science, Chemistry Department, Al Imam Mohammad Ibn Saud Islamic University (IMSIU), Riyadh 11623, KSA.

*E-mail: m_abou_krishna@yahoo.com

Received: 24 April 2015 / Accepted: 29 May 2015 / Published: 24 June 2015

Different techniques were used to illustrate the effect of manganese concentration on the composition and microstructure of Zn-Ni-Mn films. Zn-Ni-Mn alloys electrodeposited from aqueous sulfate media, under acidic conditions was investigated. According to the obtained results the Zn-Ni-Mn showed greater corrosion resistance than Zn-Ni alloy under similar conditions. Galvanostatic measurements for electrodeposition, cyclic voltammetry (CV) were used to the anodic and cathodic behavior of alloy to study the potential ranges. Anodic linear sweep voltammetry (ALSV) technique was used for the phase structure determination. It is obvious that increasing the manganese concentration results in decreasing the grain size and the coating is uniform and homogenous. The corrosion test was performed by the potentiodynamic anodic polarization method. The corrosion resistance of the coating films was increased with increasing Mn ions in the electrolyte. Under these experimental conditions the electrodeposition of the alloys is of anomalous type.

Keywords: Electrodeposition; Zn-Ni-Mn alloys; Manganese concentration; Corrosion resistance

1. INTRODUCTION

One of the most effective techniques used to protect iron and its alloys from corrosion is the electrodeposition of zinc to produce protective anticorrosive coatings on iron and its alloys. The formation of a passivation layer over the zinc surface causes a protective effect, in other words the galvanic sacrificial effect that zinc shows towards iron and its alloys [1]. In industry, zinc alloys used instead of zinc metal due to the improvement of anticorrosive properties of galvanic zinc layers on iron and its alloys [2-6]. Further laboratory studies indicated the superior anticorrosion behavior of Zn-Mn

alloys over zinc metal [7, 8], which may be attributed to the formation of a passivating layer and of Mn_2O_3 , which avoids oxygen reduction at the metallic surface. The effectiveness of the anticorrosive behavior increases with the main content of the Zn-Mn superficial alloys, although alloys with 10% Mn are already effective [7].

Manganese is much less noble than iron and is one of the few common metals with the exception of zinc and cadmium that is sufficiently active to provide sacrificial corrosion protection towards steel [9]. However, due to the high chemical reactivity and consequently the limited service life of manganese when immersed in an electrolyte or exposed outdoors [10, 11] the application of pure manganese electrodeposits as sacrificial coatings for steel has been discouraged. For corrosion resistant finishes, manganese has been mainly proposed as an alloying element, such as zinc-manganese alloys [12] which have been reported to possess the highest corrosion resistances known among zinc alloys. However, the deposition process for zinc-manganese alloys have important drawbacks, particularly with respect to the bath stability and the low cathode current efficiency CCE [12]. Therefore, there is a need for the development of new sacrificial alloy coatings. Nickel-manganese alloy electrodeposits attract interest as they potentially combine the barrier properties of Ni with the sacrificial action of manganese. Since the standard electrode potential of Ni is far from that of manganese, it is conceivable that the codeposition of manganese with nickel would be difficult. In fact, there are very few investigations reported on the electrodeposition of manganese alloys and the structure and properties of their deposits. This article will report the effect of adding manganese with various concentrations to the electrolyte bath and its effect on composition, morphology and corrosion resistance of Zn-Ni-Mn alloy films produced by electrodeposition

It is striking to mention that little work done on the electrodeposition of pure metallic manganese. The study of manganese reduction is also complicated by the fact that Mn is easily oxidized, and the manganese coatings obtained are oxidized forming a dark oxide film on the surface when they exposed to air [13]. Sulfur containing additives are commonly added to solution from which manganese is electrodeposited. It was reported [14] that the addition of such additives to the electrolytic bath leads to deposition of manganese in the brittle α -phase [15]. It was clarified that sulfur remains occluded in the coating as sulfide due to reduction of SCN^- ions during the electrodeposition process. Therefore, it is better to deposit Mn without the addition of such additives, may be with the increase of Mn electrolyte concentration.

2. EXPERIMENTAL

The standard electrolyte is composed of: H_2SO_4 [0.01 M], H_3BO_3 [0.20 M], Na_2SO_4 [0.20 M], $MnSO_4$ [0.10 M], $NiSO_4$ [0.10 M] and $ZnSO_4$ [0.10 M]. All electrolytes were freshly prepared using double distilled water and the electrodeposition done without cathode movement or solution stirring. All of the used reagent were of the best grade and were used without further purification. The $MnSO_4$ concentrations under investigation lies in 0.0 to 0.60 M range. All results were double checked and almost gave nearly the same values. The relative standard deviation (RSD%) of the standard bath deposited at different times was found to be 3.4, 2.3 and 3.2% for the Zn, Ni and Mn

contents in the deposit, respectively. Two types of cathode were used, the first (Steel rod of area 0.196 cm^2) is used for the electrochemical measurements while the second (Steel sheets of area 2 cm^2) is used for XRD analysis, chemical composition analysis and morphological properties (SEM).

Before each run, electrolytic cell [16] was cleaned with chromic/sulfuric acids mixture, then filled with 50 ml of the electroplating solution (at $25.0 \text{ }^\circ\text{C}$). EG&G Potentiostat/Galvanostat model 273A controlled by a PC using 352 corrosion software, used to perform the electrochemical measurements. Polarization resistance (R_p), corrosion potential ($E_{\text{corr.}}$) and corrosion current density ($i_{\text{corr.}}$) are the values of the electrochemical corrosion measurements of the coatings were achieved and listed in Table1.

Table 1. Values of Zn, Ni and Mn quantities in the deposit, total weight of the deposit, percentage of Zn, Ni and Mn in the deposit, current efficiencies of Zn, Ni, Mn and Zn-Ni-Mn deposits, thickness and electrochemical corrosion measurements of the deposits obtained galvanostatically at 10 mA/cm^2 and $25.0 \text{ }^\circ\text{C}$ for 10 minutes at different concentrations of MnSO_4 on steel substrate from a standard bath.

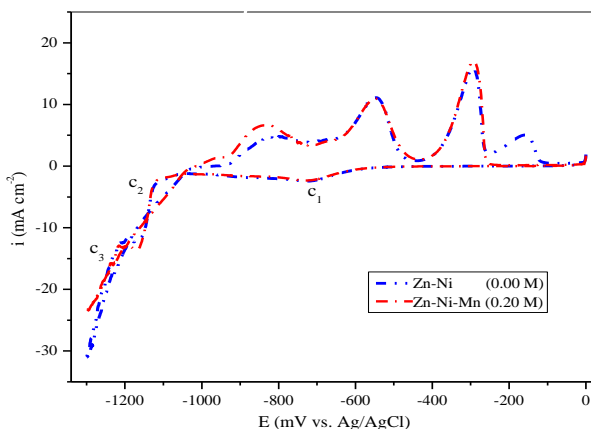
Mn concentration (M)	0.05	0.1	0.2	0.6
Parameter				
Zn amount in the deposit $\times 10^{-4} / \text{g}$	30.9	29.8	29.4	28.3
Ni amount in the deposit $\times 10^{-4} / \text{g}$	2.7	2.3	2.1	1.7
Mn amount in the deposit $\times 10^{-4} / \text{g}$	0.3	0.8	1.3	2.6
Total mass of the deposit $\times 10^{-4} / \text{g}$	33.9	32.9	32.8	32.6
Zn content / %	91.2	90.6	89.6	86.8
Ni content / %	8	7	6.4	5.2
Mn content / %	0.9	2.4	4	8
Zn current efficiency (e_{Zn}) / %	76	73.3	72.3	69.6
Ni current efficiency (e_{Ni}) / %	7.4	6.3	5.8	4.7
Mn current efficiency (e_{Mn}) / %	0.9	2.3	3.7	7.4
Zn-Ni-Mn alloy current efficiency ($e_{\text{Zn-Ni-Mn}}$) / %	84.3	81.9	81.8	81.6
Thickness of the deposit / μm	2.33	2.26	2.25	2.24
Corrosion potential ($E_{\text{corr.}}$) / mV	-820	-788	-757	-701
Corrosion current density ($i_{\text{corr.}}$) / $\mu\text{A cm}^{-2}$	34.9	30.6	25.8	18.6
Polarization resistance (R_p) / $\text{k}\Omega$	3	4.2	5.9	8.7

In cyclic voltammetry, the potential applied to the working electrode is scanned linearly back and forth one from an initial value (0.0 mV) to a second value (-1300 mV) then back to the initial value. In galvanostatic measurements, the cathodes current density is kept constant (10 mA cm⁻²) for 10 minutes. In the potentiostatic measurements, the potential of cathodes were directed by possession -1300 mV for 10 minutes.

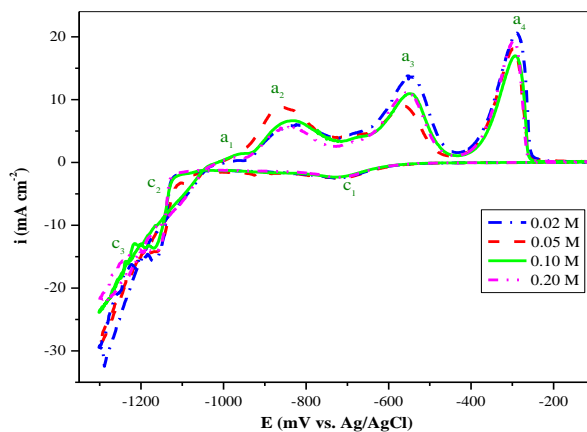
The efficiency of the process was determined from the data obtained from atomic absorption spectroscopy (Thermo scientific, model ICE 3000 series AA spectrometer) which is used to determine the chemical composition of Zn-Ni-Mn deposits. A deposited layer solution (50.0 cm³ of 25% HCl and double distilled water to a final suitable diluted) was then analyzed to find out the Zn, Ni and Mn contents in the deposited alloy and the cathode current efficiencies of pure Zn, Ni and Mn were determined [16]. The different deposited alloy phases were determined using X-ray diffraction (Bruker Axs-D8 Advance X-ray diffractometer using Cu-K α radiation). The surface morphology of the deposits was examined by Scanning Electron Microscope (JSM-5500 LV, EEM, JEOL, Japan).

3. RESULTS AND DISCUSSION

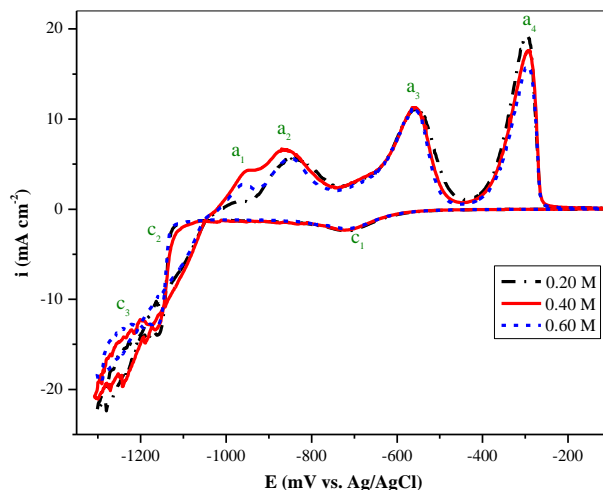
3.1. Cyclic voltammograms



A



B



C

Figure 1. *i* - *E* curves for steel at 5 mV/s and 25.0 °C in a standard Zn-Ni-Mn baths: (1a) 0.10 M MnSO₄ and 0.00 M MnSO₄, (1b) at different low concentrations of MnSO₄ and (1c) at different high concentrations of MnSO₄.

The influence of Mn²⁺ ions concentration in the electrolyte on the behavior of Zn-Ni-Mn alloys are studied firstly by cyclic voltammetry (Figures (1.a-c)). In the cyclic voltammogram of Zn-Ni (0.0 M Mn) system (Fig. 1a) the deposition reaction, starts at about -1075 mV. Previous studies have shown that zinc reduction process are controlled by mass transport [17] and sequential oxidation of different phases led to the detection of multiple peaks during the electrochemical oxidation of alloys [18]. Accordingly, the anodic sweep in Fig. 1a shows four dissolution current peaks at -822, -550, -294, and -160 mV. The first dissolution peak related to dissolution of Zn from pure Zn phase, the second peak related to dissolution of Zn from γ -Ni₅Zn₂₁ and/or δ -Ni₃Zn₂₂ phases, the third peak ascribed to the dissolution of Ni from γ -Ni₅Zn₂₁ and/or δ -Ni₃Zn₂₂ phases while the fourth dissolution peak may be attributed to the dissolution of porous Ni matrix left after the preferential dissolution of Zn from the Zn-enrich phases.

In the cyclic voltammogram of Zn-Ni-Mn at different concentrations of Mn (Fig. 1a), the deposition process starts at around -1115 mV (peak c₂), which is similar to Zn while hydrogen evolution indicated by c₃. Hence, it seems that the deposition potential dictated mainly by Zn. It is clear from the three figures (1a-c) that the cathodic peak related to the deposition of sulfur (c₁) [19] is not affected by increasing the Mn²⁺ ions concentration. However, the intensity of the cathodic peak related to the deposition of alloy components (c₂) decreases with increasing the Mn²⁺ ions concentration. It is obvious from Figure (1.a-c) that the deposition of the alloy components begins nearly at the same potential (about -1115 mV) at all concentrations except at the concentration of 0.05 M and 0.40 M where it begins at more positive potentials (-1080 mV and -1090 mV respectively).

The anodic part of the cyclic voltammograms (Figure 1b and 1c) consists of four dissolution current peaks (a_1 , a_2 , a_3 , a_4). The first peak (a_1) is attributed to the dissolution of manganese from $Mn_{0.27}Zn_{0.73}$ or ϵ -ZnMn phases (Figure 2), the second peak (a_2) is correlated to the dissolution of zinc from pure Zn phase, the third peak (a_3) is ascribed to the dissolution of zinc from γ - Ni_5Zn_{21} and/or δ - Ni_3Zn_{22} phases meanwhile the fourth peak (a_4) is related to the dissolution of nickel from Ni phases.

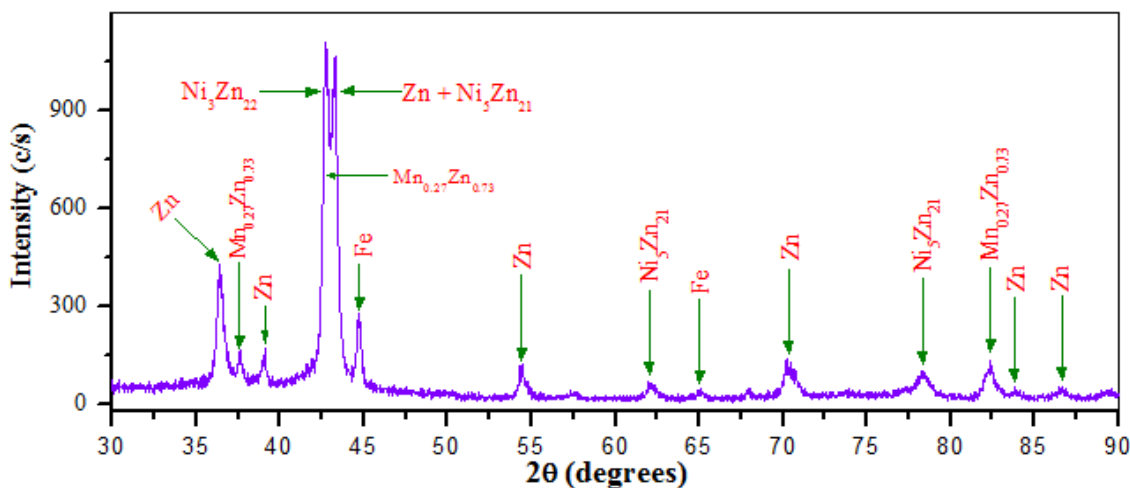


Figure 2. XRD peaks for Zn-Ni-Mn alloys electrodeposited on steel substrate of area 2 cm^2 at 10 mA cm^{-2} and $25.0\text{ }^\circ\text{C}$ from a standard bath containing 0.10 M ZnSO_4 , 0.10 M NiSO_4 , 0.10 M MnSO_4 , $0.01\text{ M H}_2\text{SO}_4$, $0.20\text{ M Na}_2\text{SO}_4$ and $0.20\text{ M H}_3\text{BO}_3$ for 10 minutes.

The height of the first peak (a_1) increases slowly as the concentration is increased from 0.02 to 0.20 M (Figure 1.b) then it increases rapidly as the concentration is increased from 0.20 to 0.60 M (Figure 1.c) where this peak becomes very obvious at the concentrations of 0.40 and 0.60 M . This gives rise to that increasing the concentration of manganese ions in the electrolyte from which the coatings are obtained is one of the methods used to obtain coatings of high manganese content. This is due to that increasing the concentration of the ions of a certain metal shift the deposition potential of this metal to more positive values. It is clear that the addition of Mn to Zn-Ni system results in the disappearance of the last anodic peak that was observed in Zn-Ni system.

In our study, manganese is the most electronegative metal and there is a significant difference between its deposition potential and the deposition potential of Zn and Ni therefore, we often obtain Zn-Ni-Mn alloys of low manganese content except at high cathodic deposition potentials and high cathodic current densities. It is clear that increasing the concentration of the ions of the less noble metal, i.e., Mn gets its deposition potential closer to that of the more noble metals i.e., Zn and Ni are resulting in obtaining alloys of higher manganese content.

As can be seen from the same three figures that the anodic current peaks (a_2 , a_3 and a_4) do not significantly change as a result of changing the Mn^{2+} ions concentration except that there are small differences between the height of the peaks. This may be because these peaks are essentially

correspond to the dissolution of Zn and Ni from their phases whose amounts do not significantly change as a result of altering the Mn^{2+} ions concentration, except at the concentration of 0.6 M as can be shown from Table (1).

3.2. Galvanostatic measurements and the anodic linear sweep voltammograms (ALSVs)

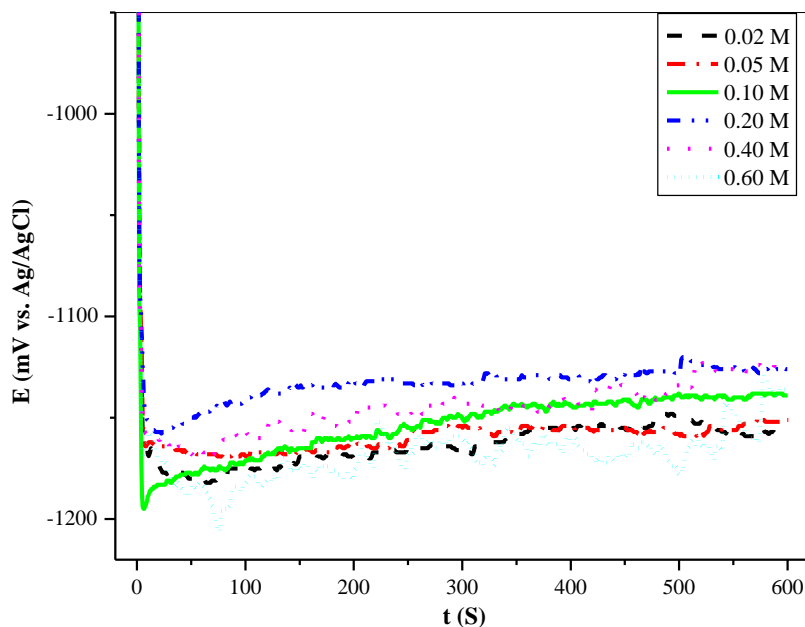


Figure 3. E - t curves for steel in a standard bath at 10 mA/cm^2 and $25.0 \text{ }^\circ\text{C}$ for 10 minutes at different concentrations of MnSO_4 .

Figure (3) shows the galvanostatic curves obtained for Zn-Ni-Mn alloys on steel rod at 10 mA/cm^2 for 10 minutes at different concentrations of Mn^{2+} ions. It is clear that the deposition potential shifts rapidly towards the negative direction during the first few seconds due to the nucleation process. The galvanostatic curves shift towards the positive direction as the concentration is increased from 0.02 to 0.20 M then they shift towards the negative direction as the concentration is increased from 0.20 to 0.60 M due to the decreases in the Ni and Zn content in the coating. There are some fluctuations in the galvanostatic curves which may be ascribed to the hydrogen evolution reaction. These fluctuations increase with increasing the Mn^{2+} ions concentration where they become maximum at the concentration of 0.60 M. These fluctuations may result in changing the composition of the deposited alloys during the growth process. At low concentrations of Mn^{2+} ions, the curves approach a stationary state after the initial times (nucleation state) resulting in the composition of the deposited coatings at these concentrations remains unchanged during the growth process.

Stripping methods are useful to determine the chemical and phase compositions of the alloys. In the case of Zn-Ni-Mn alloys, in most conditions, various peaks are observed in the oxidation scan that have been previously identified [20].

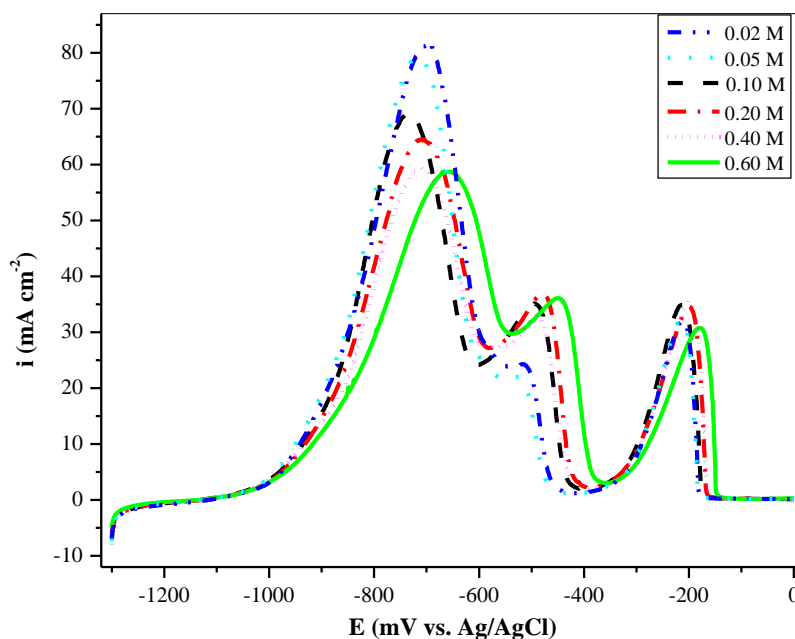


Figure 4. ALSVs for Zn-Ni-Mn alloys obtained on steel rod at 10 mA/cm^2 and $25.0 \text{ }^\circ\text{C}$ for 10 minutes at different concentrations of MnSO_4 from a standard bath, in $0.5 \text{ M Na}_2\text{SO}_4 + 0.05 \text{ M EDTA}$ at 5 mV/s and $25.0 \text{ }^\circ\text{C}$.

The anodic linear sweep voltammograms (ALSVs) obtained during the dissolution of Zn-Ni-Mn coatings (Figure 4) show the influence of Mn^{2+} ions concentrations on the phase structures of these deposited coatings. There are three anodic current peaks corresponding to the dissolution of several phases in the coatings. The first peak is attributed to the dissolution of Zn from the pure Zn phase, which is accompanied by the second peak that is related to dissolution of Zn from $\gamma\text{-Ni}_5\text{Zn}_{21}$ and/or $\delta\text{-Ni}_3\text{Zn}_{22}$ phases meanwhile the third peak is correlated to the dissolution of Ni from Ni phases. It is noteworthy that Mn does not exhibit anodic peaks during the oxidation of Zn-Ni-Mn alloys, although it exists in the alloy as clear from Table (1). Therefore, this is not due to the non codeposition of manganese but due to the overlapping between the manganese dissolution peak from its phase and the zinc dissolution peak from pure zinc phase resulting in one dissolution peak which is the first anodic current peak.

It is clear from Figure (4) that as the concentration of Mn^{2+} is increased, the first anodic peak decreases and shifted towards the positive direction due to the decreases in pure Zn amount in the deposit, but the second and third anodic peaks increase, may be due to the increase in corrosion resistance as peaks are shifted to more positive potentials. The third anodic peak start to be significantly influenced at the concentration of 0.60 M where it becomes a more positive potential.

3.3. Potentiostatic measurements and the anodic linear sweep voltammograms (ALSVs)

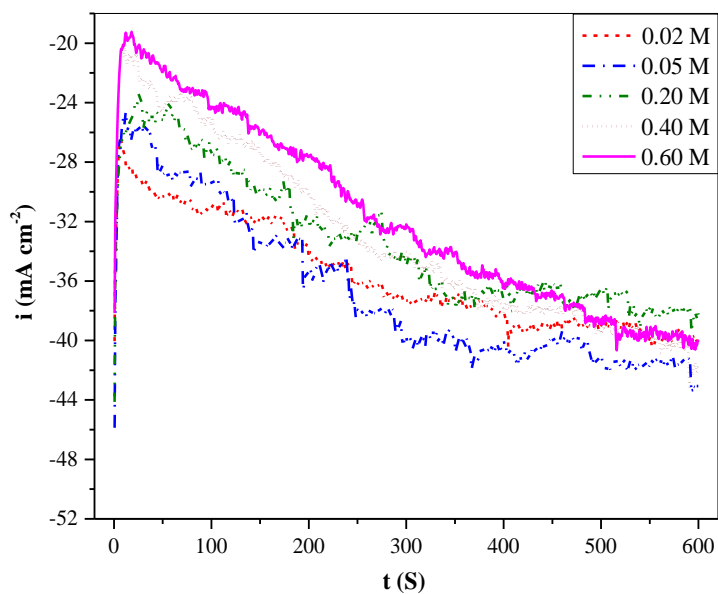


Figure 5.(a) *i* - *t* curves for steel in a standard bath at -1300 mV and 25.0 °C for 10 minutes at different concentrations of MnSO₄.

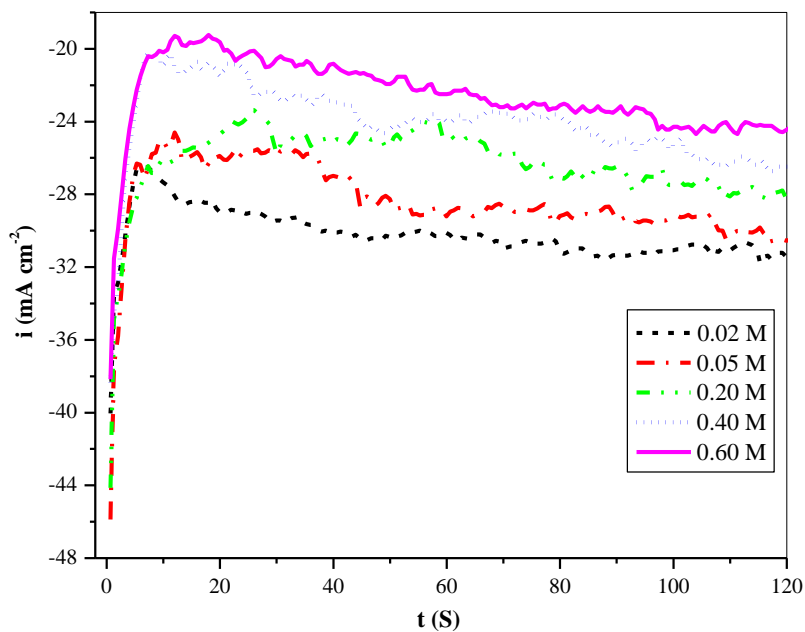


Figure 5.(b) *i* - *t* curves for steel in a standard bath at -1300 mV and 25.0 °C for 120 seconds at different concentrations of MnSO₄.

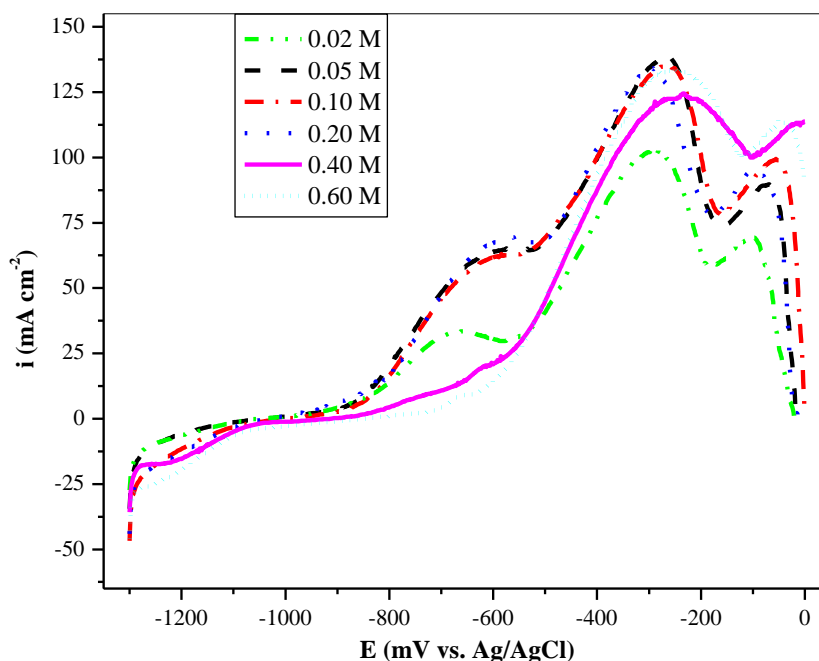


Figure 6. ALSVs for Zn-Ni-Mn alloys obtained on steel rod at -1300 mV and 25.0 °C for 10 minutes at different concentrations of MnSO_4 from a standard bath, in 0.5 M Na_2SO_4 + 0.05 M EDTA at 5 mV/s and 25.0 °C.

Figure (5.a) shows the potentiostatic current density-time curves obtained for Zn-Ni-Mn alloy on steel rod at -1300 mV for 10 minutes at different concentrations of Mn^{2+} ions. Firstly, we will illustrate these curves during the first 120 seconds (Figure (5b)) since the potentiostatic curves do not intercept with each other during this time. It is noticeable from Figure (5.b) that the current density shift rapidly to more positive values during the first few seconds due to the nucleation process. Also, the potentiostatic curves shift towards the positive direction during the first 120 seconds as the concentration of Mn^{2+} ions is increased from 0.02 to 0.60 M which may be due to the increment in the manganese content of the deposited alloy. As can be seen from Figure (5.a) at each concentration, the current density shifts towards the cathodic direction as the deposition time increases due to covering the steel substrate with Zn-Ni-Mn coating. It is clear that the potentiostatic curves intercept with each other after the first 120 seconds. There are fluctuations of low frequency and magnitude in the potentiostatic curves which may be attributed the hydrogen evolution reaction or the formation of dendritic deposits [15].

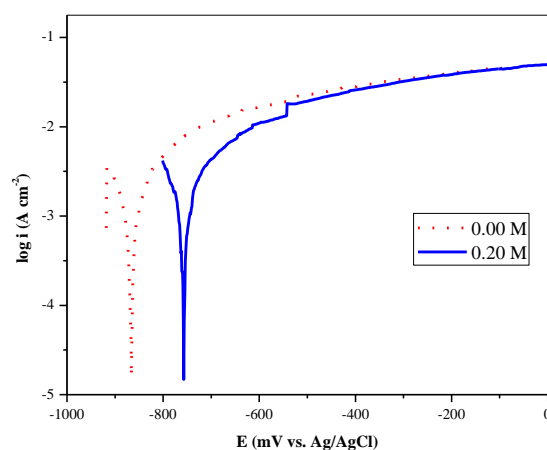
Figure (6) shows the ALSVs obtained during the dissolution of Zn-Ni-Mn alloys electrodeposited at -1300 mV for 10 minutes at different concentrations of Mn^{2+} ions. At the concentrations ranging from 0.02 to 0.20 M, there are three anodic current peaks which are ascribed to the dissolution of the alloy components from their different phases as previously discussed. It is obvious that the ALSVs at the concentrations of 0.02, 0.05 and 0.20 M have similar trends, where all the anodic peaks are close to each other with respect to their heights and their potentials. This refers to the similar composition of the

coatings obtained at these concentrations. At the concentration of 0.10 M, there is a clear decrease in the height of all peaks, moreover the peaks slightly shift towards the negative direction where they become at less noble potentials.

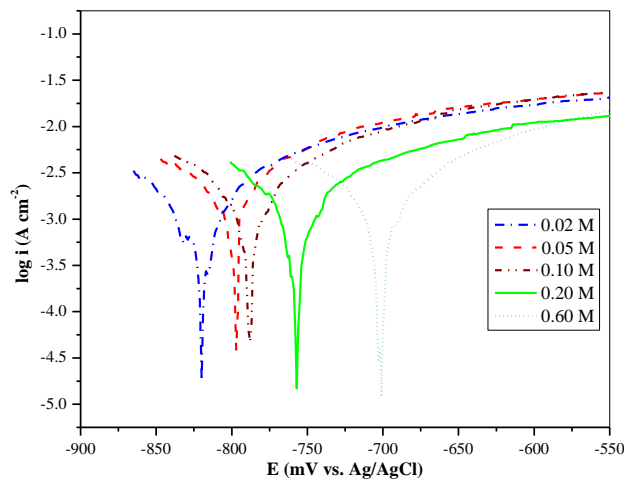
It is striking that the coatings obtained at high manganese concentrations, i.e., 0.40 and 0.60 M has abnormal dissolution behavior where there is a sharp decrease in the height of the first dissolution peak resulting in overlapping with the second peak. This refers to the lower content of the pure Zn phase obtained at these concentrations. Furthermore, the current density does not reach zero at the end of the oxidation process indicating that the deposit is not completely removed from the electrode surface. This gives rise to the excellent corrosion resistance properties for the coatings obtained at high concentrations of Mn^{2+} ions.

On comparing the ALSVs obtained in Figure (4) and Figure (6), we can conclude the following: firstly, the peaks produced from the oxidation of the coatings electrodeposited under potentiostatic conditions at different concentrations of manganese ions are at more noble potentials than those electrodeposited under galvanostatic conditions at the same concentration. Secondly, the first anodic peak in the ALSVs produced from the oxidation of the coatings electrodeposited under galvanostatic conditions is higher than the other two peaks. In the meantime, the first anodic peak in the ALSVs produced from the oxidation of the coatings electrodeposited under potentiostatic conditions is lower than the other two peaks. This refers that the coatings obtained under galvanostatic conditions contain higher quantities of pure Zn phase and lower quantity of $\gamma\text{-Ni}_5\text{Zn}_{21}$ and/or $\delta\text{-Ni}_3\text{Zn}_{22}$ phases than those obtained under potentiostatic conditions at the same concentration. This indicates the better corrosion resistance properties of the coatings obtained potentiostatically than those obtained galvanostatically at the same manganese ions concentration. Finally, it is clear from the two figures that the influence of altering the manganese ions concentration on the composition and properties of the coatings obtained under potentiostatic conditions is more than the coatings obtained under galvanostatic conditions.

3.4. The potentiodynamic polarization measurements



A

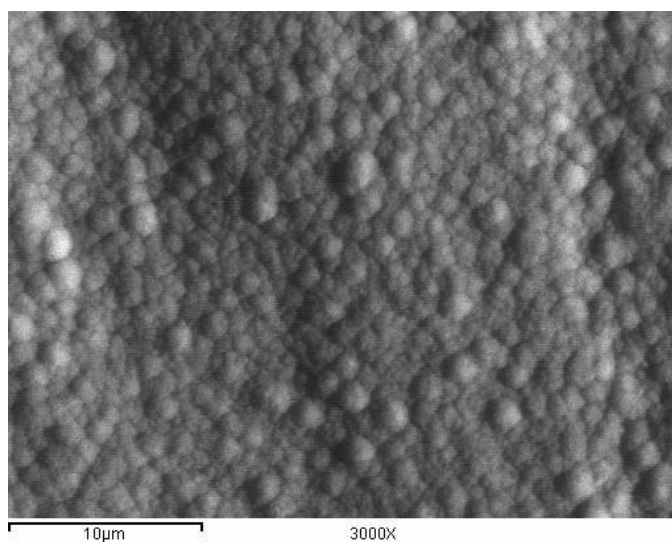


B

Figure 7. $\log i - E$ curves for Zn-Ni-Mn alloys obtained on steel rod at -1300 mV and 25.0 °C for 10 minutes, (7a) at 0.10 M MnSO_4 and 0.00 M MnSO_4 and (7b) at different concentrations of MnSO_4 from a standard bath, in 0.05 M HCl at 5 mV/s and 25.0 °C.

Figure (7 a and b) exhibits the potentiodynamic polarization curves for Zn-Ni-Mn alloys obtained potentiostatically at -1300 mV for 10 minutes over a steel rod at different concentrations of Mn^{2+} ions [21]. It is noticeable that the deposits have more negative corrosion potentials at the concentrations of 0.00 , 0.02 , 0.05 and 0.10 M than at the concentrations of 0.20 and 0.60 M. These results are in agreement with the results obtained from ALSVs (Figure 6). It is clear that the coating possesses the highest corrosion resistance properties at the concentration of 0.60 M which may be correlated to the increase in the content of $\gamma\text{-Ni}_5\text{Zn}_{21}$ and/or $\delta\text{-Ni}_3\text{Zn}_{22}$ phases.

3.5. The scanning electron microscopy (SEM)



8 (a)

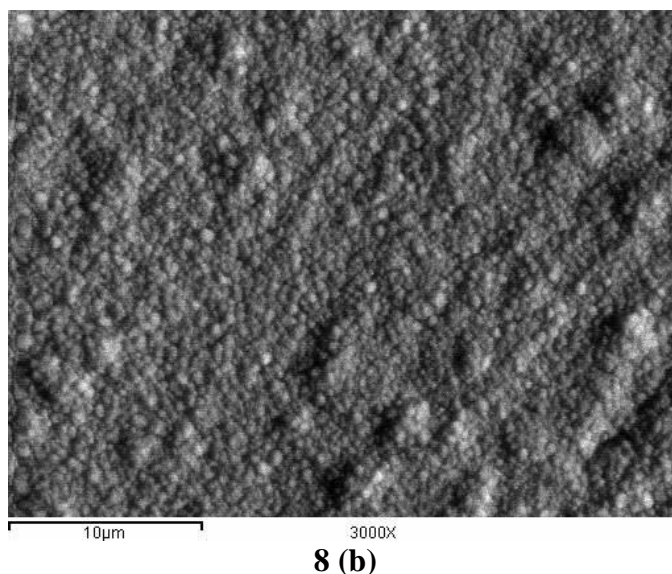


Figure 8. (a and b) SEM micrograph (at magnification of 3000 \times) for Zn-Ni-Mn alloy electroplated on steel substrate of area 2 cm² at 10 mA/cm² and 25.0 °C for 10 minutes from a standard bath at different concentration of MnSO₄ (a) 0.01 M and (b) 0.60 M MnSO₄.

Figures (8.a and b) show the scanning electron microscopy (SEM) micrographs for Zn-Ni-Mn alloys obtained on steel substrate at 10 mA/cm² and 25.0 °C for 10 minutes at Mn concentrations of 0.10 and 0.60 M. It is obvious that increasing the manganese concentration results in decreasing the grain size and the coating are uniform and homogenous. As can be shown from the figures, the coatings completely cover the substrate and there are no cracks.

3.6. Electrochemical measurements and chemical analysis

Table (1) illustrates the dependence of Zn-Ni-Mn alloy composition on the manganese ions concentration in the electrolyte from which the alloys are obtained. It is clear that the content of Zn decreases from 91.2% to 86.8%, meanwhile the content of Mn increases from 0.9% to 8% as the concentration is increased from 0.05 to 0.60 M. The content of Ni decreases from 8% to 5.2% as the concentration is increased from 0.05 to 0.60 M. This indicates that the decrease in Zn and Ni contents at high concentrations of manganese ions is replaced by an increment in the Mn content. Also, the obtained results represented in Table (1) demonstrate the dependence of the current efficiency of Zn, Ni and Mn metals and Zn-Ni-Mn alloy on the manganese ions concentration in the electrolyte from which the alloys are obtained. As can be shown, the efficiency of Zn and Ni increases as the concentration is decreasing as the concentration is increased from 0.05 to 0.60 M. The efficiency of Mn increases from 0.9% to 7.4% as a result of increasing the concentration from 0.05 to 0.60 M. The alloy efficiency decreases from 84.3% to 81.6% as a result of increasing the concentration from 0.05 to 0.60 M. The decrease in the alloy efficiency at high concentrations of Mn²⁺ ions can be ascribed to the increment in the hydrogen evolution reaction which completes the efficiency to 100%. The results clarify that the thickness of the deposited coating decreases as the concentration is increased. The

decrease in the coating thickness at high concentrations of Mn^{2+} ions is perhaps related to the decrease in the Zn content which represents the main alloy component of low density.

The obtained results (Table 1) indicated that the thickness of the layer decreases as Mn^{2+} concentration increases due to that the Zn content decreases and the maximum polarization resistance and the lowest corrosion current and the more positive corrosion potential of the deposit was attained at 0.60 M [22].

4. CONCLUSION

This division includes the influence of Mn^{2+} ions concentration in the electrolyte on the composition, structure, appearance, morphology and corrosion resistance properties of the deposit. The cathodic peak related to sulfur deposition is not influenced by increasing the Mn^{2+} ions concentration. The excellent corrosion resistance properties of the obtained coatings are at high concentrations of Mn^{2+} ions (0.40 and 0.60 M). It has been concluded that the influence of altering the manganese ions concentration on the composition and properties of the coatings obtained under potentiostatic conditions is more than its influence on the composition and properties of the coatings obtained under galvanostatic conditions. Furthermore, the corrosion resistance properties of the coatings obtained potentiostatically are better than those obtained galvanostatically at same manganese ions concentration.

Increasing the manganese concentration results in decreasing the grain size and the coating is uniform and homogenous. Increment the Mn^{2+} ions concentration from 0.1 to 0.6 M results in increasing the Mn content meanwhile the Zn and Ni contents decrease. The decrease in the alloy efficiency at high concentrations of Mn^{2+} ions can be ascribed to the increment in the hydrogen evolution reaction which completes the efficiency to 100%. The decrease in the coating thickness at high concentrations of Mn^{2+} ions is perhaps related to the decrease in the Zn content which represents the main alloy component of low density.

References

1. P. Brito, L. Rodrigues, T. Nabais, C. Sequeira, D. Santos, "Corrosion behaviour of Zn electrodeposits from spent Zn–MnO₂ batteries", Eurocorr 2007, Freiburg, Germany, 2007.
2. H. A. Conrad, M. R. McGuire, T. Zhou, M. I. Coskun and T. D. Golden, *Surf. Coat. Technol.* 272 (2015) 50.
3. K. O. Nayana, *Bullet. Mater. Sci.* 37 (2014) 1137.
4. A. Tozar, *Appl. Surf. Sci.* 318 (2014): 15.
5. Z. Feng, Q. Li, J. Zhang, P. Yang, H. Song and M. An, *Surf. Coat. Technol.* 270 (2015) 47.
6. S. Ghaziof and W. Gao, *Appl. Surf. Sci.* 311 (2014) 635.
7. N. Boshkov, *Surf. Coat. Technol.* 172 (2003) 217.
8. D. Sylla, C. Savall, M. Gadouleau, C. Rebere, J. Creus and P. Refait, *Surf. Coat. Technol.* 200 (2005) 2137.
9. A. Brenner, *Electrodeposition of Alloys*, Vol. I, p. 137, Academic Press, New York 1963.
10. J. Gong and G. Zangari, *J. Electrochem. Soc.* 149 (2002) 2002.

11. J. Gong, I. Zana and G. Zangari, *J. Mater. Sci. Lett.* 20 (2001) 1921.
12. C. Müller, M. Sarret and T. Andreu, *J. Electrochem. Soc.* 149 (2002) 600.
13. P. Díaz-Arista, R. Antaño-López, Y. Meas, R. Ortega, E. Chainet, P. Ozil and G. Trejo, *Electrochim. Acta*, 51 (2006) 4393.
14. J. E. Lewis, P. F. Scaife and D. A. Swinkels, *J. Appl. Electrochem.* 6 (1976) 199.
15. D. Sylla, J. Creus, C. Savall, O. Roggy, M. Gadouleau and Ph. Refait, *Thin Solid Films* 424 (2003) 171.
16. M. M. Abou-Krishna, *Appl. Surf. Sci.* 252 (2005) 1035.
17. P. Díaz-Arista, Y. Meas, R. Ortega and G. Trejo, *J. Appl. Electrochem.* 35 (2005) 217.
18. G. Trejo, R. Ortega, Y. Meas, E. Chainet and P. Ozil, *J. Appl. Electrochem.* 33 (2003) 373.
19. M. M. Abou-Krishna, H. M. Rageh and E. A. Matter, *Surf. Coat. Technol.* 202 (2008) 3739.
20. J. B. Bajat, M. D. Maksimović and G.R. Radović, *J. Serb. Chem. Soc.* 67 (2002) 625.
21. K. R. Baldwin and C. J. E. Smith, *Trans. IMF* 74(1996) 202.
22. E. Chassaing, K. Vu Quang and R. Wiart, *J. Appl. Electrochem.* 19(1989) 839.

© 2015 The Authors. Published by ESG (www.electrochemsci.org). This article is an open access article distributed under the terms and conditions of the Creative Commons Attribution license (<http://creativecommons.org/licenses/by/4.0/>).